Materials and Structures (2024) 57:89
https://doi.org/10.1617/s11527-024-02352-8

ORIGINAL ARTICLE

Experimental characterization of bond between concrete and HDG steel tubes for mixed steel-concrete structures

Fábio Cruz · Isabel Valente · João Almeida · Ana Neves · Eduardo Pereira

Received: 16 October 2023 / Accepted: 9 April 2024 / Published online: 3 May 2024
© The Author(s) 2024

Abstract Bond between concrete and reinforcement material is crucial for the structural behaviour and design of reinforced concrete or mixed steel-concrete structures. When considering applications in harsh environments, such as severe marine exposure or submerged conditions, hot-dip galvanized (HDG) steel seems to be a promising solution, as part of new mixed steel-concrete structural systems. Although it is essential to guarantee an effective composite response, the interaction and bond behaviour between materials is not yet sufficiently well understood. This experimental investigation aimed to study the bond behaviour between concrete and HDG steel tubes, including the influence of adopting concrete pin connectors by creating holes in the tube profile, and also the influence of the galvanic surface state. The impact of bond length on the bond behaviour of the galvanized steel tube embedded in different concrete mixtures was analysed. Pushout tests were conducted to obtain the load end *versus* slip responses, as well as the failure modes. The results showed that the embedment lengths and the concrete compositions had no relevant effect on the overall shape of the pushout experimental responses, with the exception of the specimens that include the concrete pin connector. However, both variables clearly influenced the bond stress, dissipated energy during pushout until failure, and residual pushout force. The addition of the concrete pin significantly improved the adherence mechanism, while the contamination of the galvanic surface showed to significantly reduce the bond strength.

Keywords HDG steel · Concrete · Plain tubes · Bond behaviour · Pushout tests

F. Cruz (✉) · I. Valente · J. Almeida · A. Neves · E. Pereira
Department of Civil Engineering, ISISE, Institute of Science and Innovation for Bio-Sustainability (IB-S), University of Minho, 4800-058 Guimarães, Portugal
e-mail: id8024@alunos.uminho.pt

I. Valente
e-mail: isabelv@civil.uminho.pt

J. Almeida
e-mail: j.almeida@civil.uminho.pt

A. Neves
e-mail: id6951@alunos.uminho.pt

E. Pereira
e-mail: eduardo.pereira@civil.uminho.pt

1 Introduction

Coastal and offshore marine structures are exposed to severe exposure conditions and, consequently, present durability problems due to physical, chemical and microbiological deterioration [1–3]. This reduces its service life and increases the maintenance costs [4, 5].

Corrosion is a major cause of structural degradation and the main cause of structural failure [6–8]. Although this cannot be completely eliminated, the use of suitable protection systems, such as cathodic

protection or corrosion inhibitors may limit corrosion and minimize durability problems [9, 10]. Nevertheless, these are expensive and may not always be applied due to its potentially environmental negative impact [11]. In particular, some inhibitors may cause significant deterioration in the mechanical properties of concrete. On the other hand, the use of coating products on steel presents itself as a protective method since it can prevent the direct contact of steel with oxygen, carbon dioxide, chlorides and moisture [12, 13]. In this context, the use of a hybrid structure combining concrete and hot-dip galvanized (HDG) steel is regarded as a promising solution [6, 9, 14, 15]. Concrete and HDG steel, in the form of tube profiles, may be used in marine constructions such as floating or submerged structures including artificial reef structures [2], submarine pipelines, offshore wind turbine towers and bridge piers, some in the form of concrete-encased steel elements or concrete-filled steel tubular (CFST) members [16, 17].

The coating also guarantees the preservation of the mechanical properties of steel and does not require periodic maintenance, even in the harshest environments. However, despite all the advantages, it influences the bond behaviour between the steel and concrete [6, 9, 12, 18, 19].

The bond stress-slip relationship characterizes the steel-concrete interface behaviour and may be obtained experimentally using direct pushout or pull-out tests, and indirectly through flexural tests [9, 18].

The bond behaviour between galvanized steel and concrete is determined by the chemical bond strength between steel and the cement (chemical adherence), and depends on the relative displacement between the two surfaces (friction) and interlocking mechanisms (mechanical adherence).

Corrosion and galvanization can significantly influence the chemical bond between steel reinforcement and concrete, namely due to the reaction between galvanized coating and the cement paste, as well as the influence of corrosion on bond behaviour over time. Previous studies revealed inconclusive results [6, 9, 18, 20–22]. According to several authors, the galvanized steel surface is activated when in contact with fresh concrete due to its alkaline nature [22, 23]. During the curing process, the zinc coating corrodes until passivation occurs. At this early stage, rapid corrosion of the coating may result in the removal of a significant amount of this layer, thus resulting in poor protection. Simultaneously, as a result of the cathodic reaction, hydrogen production occurs, which increases the porosity of the concrete and consequently decreases the chemical bond between the materials [9, 23–25]. Sanz et al. (2017) found that the corrosion depth did not impact the maximum shear stress, suggesting consistent adherence in all specimens. Yet, the corrosion depth does influence residual stress, revealing a detectable dilatant behaviour. In contrast, according to Yeomans (2004), zinc corrosion products have the ability to migrate from the surface of galvanized reinforcement to the concrete matrix, reducing the likelihood of concrete corrosion-induced damage. Also, galvanized steel may be exposed to chloride ion concentrations at least 4–5 times higher than steel and remain passivated at a lower pH than regular steel [23]. The combination of these two factors is commonly accepted as the basis for the superior performance of galvanized reinforcement compared to uncoated steel. Ortolan et al. (2017) indicates that mixtures with a lower water/cement ratio, and therefore with greater strength, favour the use of galvanized steel [25].

While conventional galvanization of reinforcing steel extends the service life of reinforced concrete structures and has a clearly superior carbonation resistance, recent investigations show that it may result in decreased bond between steel and concrete, with negative consequences for the bearing capacity of structures [9]. On the other hand, some authors claim that its influence is negligible [26] and further studies are therefore required to investigate in detail the bond behaviour between HDG steel and concrete [27]. Thus, this experimental research aimed at characterizing the influence of the bond length, the concrete mixture, the pin connector and the surface contamination on the HDG steel – concrete bond behaviour by direct pushout tests.

2 Experimental program

In order to study the bond between HDG steel and concrete, an experimental program was devised, based on pushout tests, to evaluate the influence of the bond length (LB) and the concrete mixture (MXX). The experimental program was composed of 40 tests divided into four groups (I, II, III and IV) according to the concrete mixture developed. For

each, three different series, according to the LB, were considered.

The chosen LBs were evaluated using expressions 6.9–4 to 6.9–6 of CEB-FIP model code 90 [28]. For that, the design bond stress considered the concrete tensile strength, smooth surface of the reinforcement bar, bad adherence with the concrete matrix and the tube diameter. The bond length required to anchor the tensile force installed in the tube was calculated assuming constant tension in the tube loaded end section and the mechanical properties of the steel used, leading to an LB equal to 1281.11 mm (considering C30/37). Note that, when considering the experimental bond stress obtained by Sanz et al. (2017), the LB would be 176.72 mm. Therefore, to have debonding failure during testing, three LB values (50, 75 e 150 mm), smaller than the effective bond length and compatible with the concrete cube dimensions, were adopted.

The following nomenclature was adopted for the specimens: MXX_LBYY_ZZ; where XX identifies the concrete mixture number, YY identifies the bond length in millimetres and ZZ designates the number of the specimen tested adopting the same testing conditions (Table 1).

To understand the influence of concrete strength and cement content on the bonding properties, the three tested concrete compositions represented common low to medium strength concretes. An additional series of tests was included in group III with the suffix designation H40, suggesting "hole of 40 mm", in order to study the concrete pin on the bond behaviour. In this case the LB of 100 mm was adopted. These holes allowed the continuity between the inner and outer regions of the tube, which may be of interest for mixed concrete–HDG steel construction systems.

A total of 32 concrete cylinders were tested to characterize its mechanical properties at 7 and 28 days after casting. Moreover, 4 steel samples were extracted from the HDG steel in order to assess its mechanical properties.

It should also be noted that the specimens of group IV were constructed by reusing the tubes tested in group I and were not cleaned, in order to evaluate the importance of a clean HDG surface on the results compared with group III.

Table 1 Variables and specimens tested in the experimental program

Concrete	LB [mm]	No. of specimens	Series
M01	50	3	M01_LB50_01 to 03
	75	3	M01_LB75_01 to 03
	100	4	M01_LB100_01 to 04
M02	50	3	M02_LB50_01 to 03
	75	3	M02_LB75_01 to 03
	100	3	M02_LB100_01 to 03
M03	50	3	M03_LB50_01 to 03
	75	3	M03_LB75_01 to 03
	100	3	M03_LB100_01 to 03
	100	3	M03_LB100_H40_01 to 03
M04 ("reused" tubes)	50	3	M04_LB50_01 to 03
	75	3	M04_LB75_01 to 03
	100	3	M04_LB100_01 to 03

2.1 Materials

Concrete composition requirements included a good workability in the fresh state to guarantee the appropriate filling of the moulds, characteristics that promote the durability of the structural systems, and strength and deformability properties in the hardened state comparable to the most common ones in the type of applications studied. One of the initial consequences of these requirements is the need to use small size aggregates, which allow concrete to flow without any constraint, particularly in M03_LB100_H40. The concrete compositions developed using the modified equations proposed by Andreasen & Andersen [29] are shown in Table 2.

2.2 Geometry and preparation of specimens

The test specimens consisted of concrete cubes of $150 \times 150 \times 150$ mm^3, where HDG steel tubes with a total length of 200 mm were embedded, at LB of 50 mm, 75 mm or 100 mm. In order to accurately guarantee these LB, circular pieces of polystyrene foam with different thicknesses were placed under the tubes before casting. To guarantee the correct positioning of the tubes, steel frames were attached to the moulds (Fig. 1). Casting was carried out cautiously, to avoid HDG steel tube surface contamination with products that could alter the bond behaviour. After two days, the concrete cylinders and the pushout specimens were placed in a climatic chamber at $58 \pm 2\%$ of relative

Table 2 Concrete composition

Materials	Mixture 1 [kg/m^3]	Mixture 2 [kg/m^3]	Mixture 3 & 4 [kg/m^3]
CEM II/A-L 42,5R	230.0	350.0	450.0
Limestone filler	108.0	0.0	0.0
Fine sand 0/2	338.8	335.0	294.5
Fine sand 0/4	853.0	845.0	750.0
Gravel aggregate 6/14	637.2	625.0	558.0
Superlasticizer masterease 3530	1.6	1.6	1.6
Plasticizer masterpozzolith 476N	1.6	1.6	1.6
Water	157.2	157.0	201.8
w/c	0.684	0.449	0.449

Fig. 1 Specimen's preparation

humidity (RH) and 20 ± 1 °C of temperature (*T*). Prior to the tests, the foam was removed and the air gap was measured. Before assembling the specimens, the HDG steel tubes were cleaned following the recommendation of the American Galvanizers Association [30], to remove organic contaminants resulting from handling, cutting and transportation processes. For this, a mild alkaline solution with ten parts water and one part of alkaline cleaner was used.

2.3 Testing methods

2.3.1 Concrete properties

The fresh properties of the concrete mixtures were evaluated by performing the slump test with the Abrams cone, following the European Standard EN 12350-2 [31]. The compressive behaviour was characterized by means of uniaxial compression tests

Table 3 Slump flow and mechanical properties of concrete mixtures 1 to 4

	Slump class	$E_{cm,7d}$ [GPa]	$f_{cm,7d}$ [MPa]	$E_{cm,28d}$ [GPa]	$f_{cm,28d}$ [MPa]
M01	S1	23.57	16.99	22.70	20.44
		[0.30%]	[2.23%]	[6.16%]	[2.88%]
M02	S4	26.24	26.11	28.10	31.17
		[3.54%]	[11.12%]	[1.44%]	[4.66%]
M03	S4	28.85	34.38	28.20	37.89
		[0.07%]	[1.12%]	[2.25%]	[0.91%]
M04	S4	26.97	36.81	28.03	43.27
		[1.32%]	[0.90%]	[0.92%]	[1.22%]

in cylinders with 150 mm diameter and 300 mm in height [32]. Young's modulus (E_{cm}) and compressive strength (f_{cm}) of concrete were assessed according to EN 12390-13 [33] and EN 12390-3 [34].

Table 3 shows the average results obtained for concrete characterization. In general, the mixtures showed good consistency and workability with no segregation, i.e. the separation of the liquid from the solid phase. Mixture M01, M02, M03 and M04 may be characterized by a strength class C12/15, C20/25, C30/37 and C35/45, respectively [35].

2.3.2 HDG steel properties

According to the manufacturer, the HDG steel tubes belong to the light series with a mean external diameter of 88.61 mm (CoV = 0.04%) and a mean average thickness of 3.08 mm (CoV = 0.86%).

According to EN 10255, it corresponds to steel with a yield strength exceeding 195 MPa, ultimate tensile strength between 320 and 520 MPa, and an ultimate tensile strain exceeding 20%.

In order to characterize the mechanical properties of the HDG steel, four uniaxial tensile tests were performed based on ISO 6892-1 [36]. The applied tensile load and the strain in the longitudinal axis at middle height were measured. The modulus of elasticity (E), the elongation (A), the tensile strength (Rm) and the upper yield strength (R_{eH}) or proof strength (R_p) were obtained.

Note that, according to the manufacturer, R_{eH} is equal to 289 MPa. However, since the experimental responses obtained in tension do not clearly exhibit a yielding plateau, the proof strength corresponding to 0.2% of strain ($R_{p0,2}$) was obtained instead. Figure 2 presents the steel uniaxial stress-strain curves and properties. The tested steel showed typical behaviour and rupture of the material.

2.3.3 Pushout tests

Considering the configurations and dimensions found in the literature [7, 10, 18, 37], a concrete prism with 150 mm was adopted, in order to reduce the material waste and weight of the specimen. Supportive numerical analysis [38] were carried out to check the test configuration and ensure that the tensile strength of the surrounding concrete was not exceed by the circumferential stresses generated when the pushout force is transferred from the tube (action) to the block (reaction). The results showed that the stress distribution was satisfactory to the debonding phenomenon.

Figure 3 shows the test setup adopted on the experimental program. The test consisted on subjecting the steel tubes to an uniaxial compressive force. The specimen was positioned on a rigid metal piece connected to a steel reaction frame. An angular spherical bearing was used at the loading section to provide stability and facilitate initial system adjustment. The specimens were tested at a loading rate of 2 μm/s until a constant residual force was reached, based on previous studies [17, 18, 24, 27, 37]. A servo-hydraulic equipment with 100 kN (±0.12 kN; 0.05% F.S.) maximum load capacity was used. A linear variable differential transducer (LVDT1) with a stoke of ± 10 mm (linearity error of 0.24% F.S.) was used to control the test. LVDT 2, 3 and 4, positioned 120º from each other, with a stoke of ± 10 mm were used to measure the relative displacement between the tube and the concrete at the loaded end section. LVDT 5 with a stoke of ± 5 mm was used at the at the free end section.

Although the bond shear stress (τ) presents an uneven distribution following a nonlinear shape along the anchorage length, an average shear stress was assumed for evaluation and comparison purposes, following the approach typically adopted in the design codes. Thus, τ_{max} was computed as shown in Eq. (1).

$$\tau_{max} = \frac{F_{l,\max}}{\pi \times D \times \left(\mathrm{LB} - S_{l,\max}\right)} \quad (1)$$

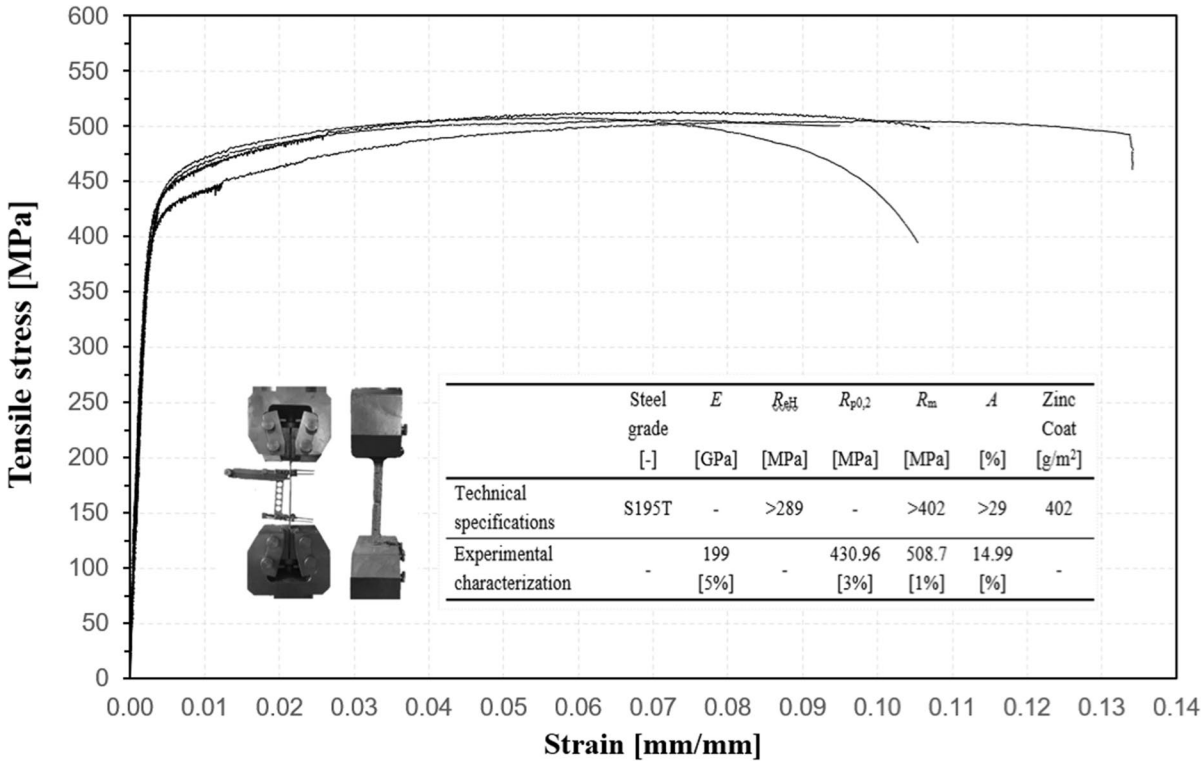

	Steel grade [-]	E [GPa]	R_{eH} [MPa]	$R_{p0,2}$ [MPa]	R_m [MPa]	A [%]	Zinc Coat [g/m²]
Technical specifications	S195T	-	>289	-	>402	>29	402
Experimental characterization	-	199 [5%]	-	430.96 [3%]	508.7 [1%]	14.99 [%]	-

Fig. 2 HDG steel uniaxial stress-strain curves and properties

where $F_{l,\max}$ is the maximum pushout load, D is the outer diameter of the steel tube, LB is the bond length, and $s_{l,\max}$ is the displacement of the tube at the loaded end section corresponding to $F_{l,\max}$.

3 Results and discussion

3.1 Bond behaviour

Figure 4 presents the amplification of the initial part of the typical experimental curve in terms of pushout force (F_l) versus loaded end slip (s_l) and free end slip (s_f). The loaded end slip curve allowed to discern the starting of the tube slip. In contrast, the sliding of the free end was initiated only at the final stage of the debonding experimental responses. Figure 5 shows the experimental responses obtained in terms of (F_l–s_l), at the loaded end zone. F_l was measured by the load cell of the actuator, and the s_l was obtained by averaging the measurements taken from the three LVDTs 2, 3 and 4.

The experimental responses obtained are divided according to mixtures. In general, the F_l-s_l experimental responses exhibit a very similar global behaviour for all specimens. The responses are essentially marked by three distinct phases, regardless of the type of concrete used and the LB adopted. Initially an elastic behaviour phase is observed (pre-peak branch), due to the contribution of the chemical bond between concrete and the surface of the HDG steel, which results in the perfect bond between the two materials involved. The system shows a high initial stiffness, with a progressive increase of the load capacity for a very low s_l, until the peak pushout force is reached. After this first phase, the specimens exhibit a nonlinear F_l–s_l experimental response, that is characterized by a very fast reduction of the load carrying capacity and the loss of stiffness due to bond degradation (post-peak branch). It should also be noted that the transition between the pre-peak phase and the post-peak softening phase happens smoothly due to the progressive propagation of the detachment crack that breaks the chemical bond, and due to the remaining

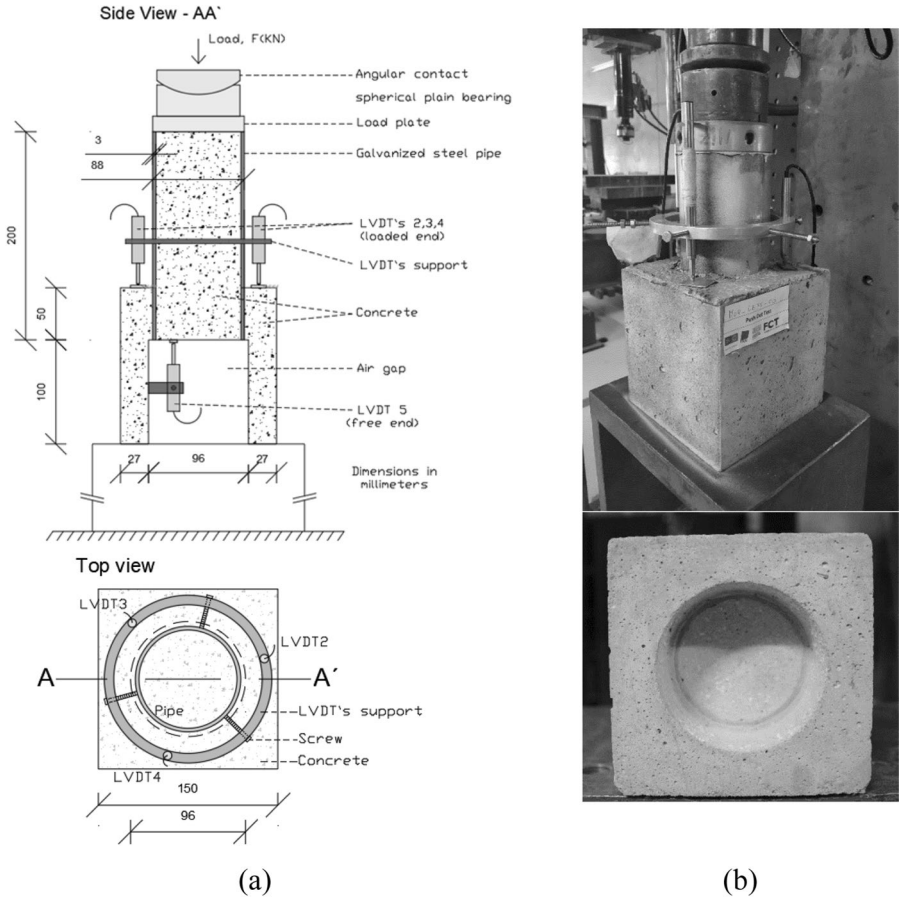

Fig. 3 Experimental setup and instrumentation adopted for pushout tests

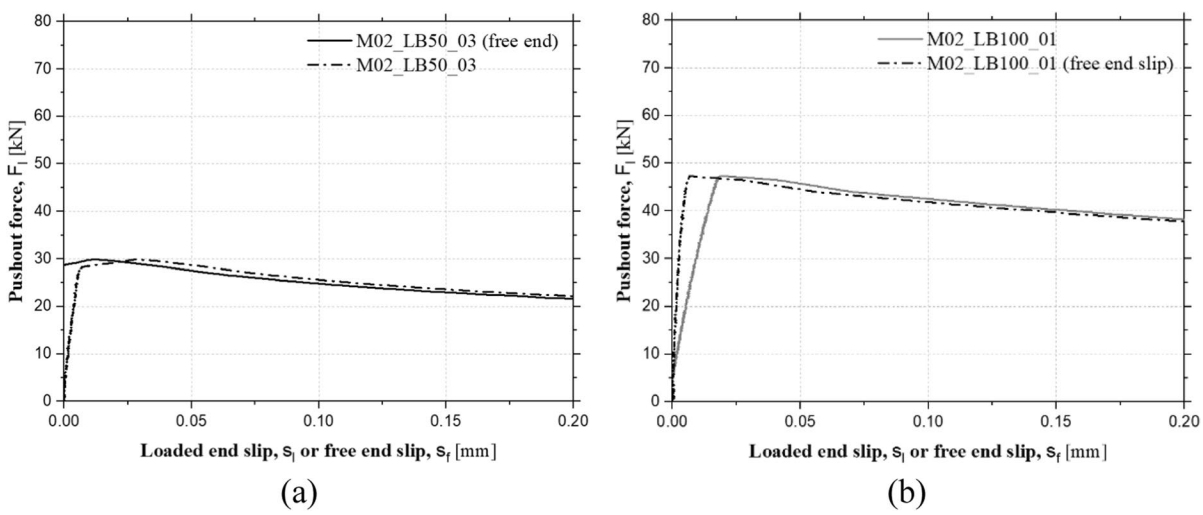

Fig. 4 Typical responses in terms of $F_l - s_l$ and $F_l - s_f$: **a** M02_LB50_01 and **b** M02_LB100_01

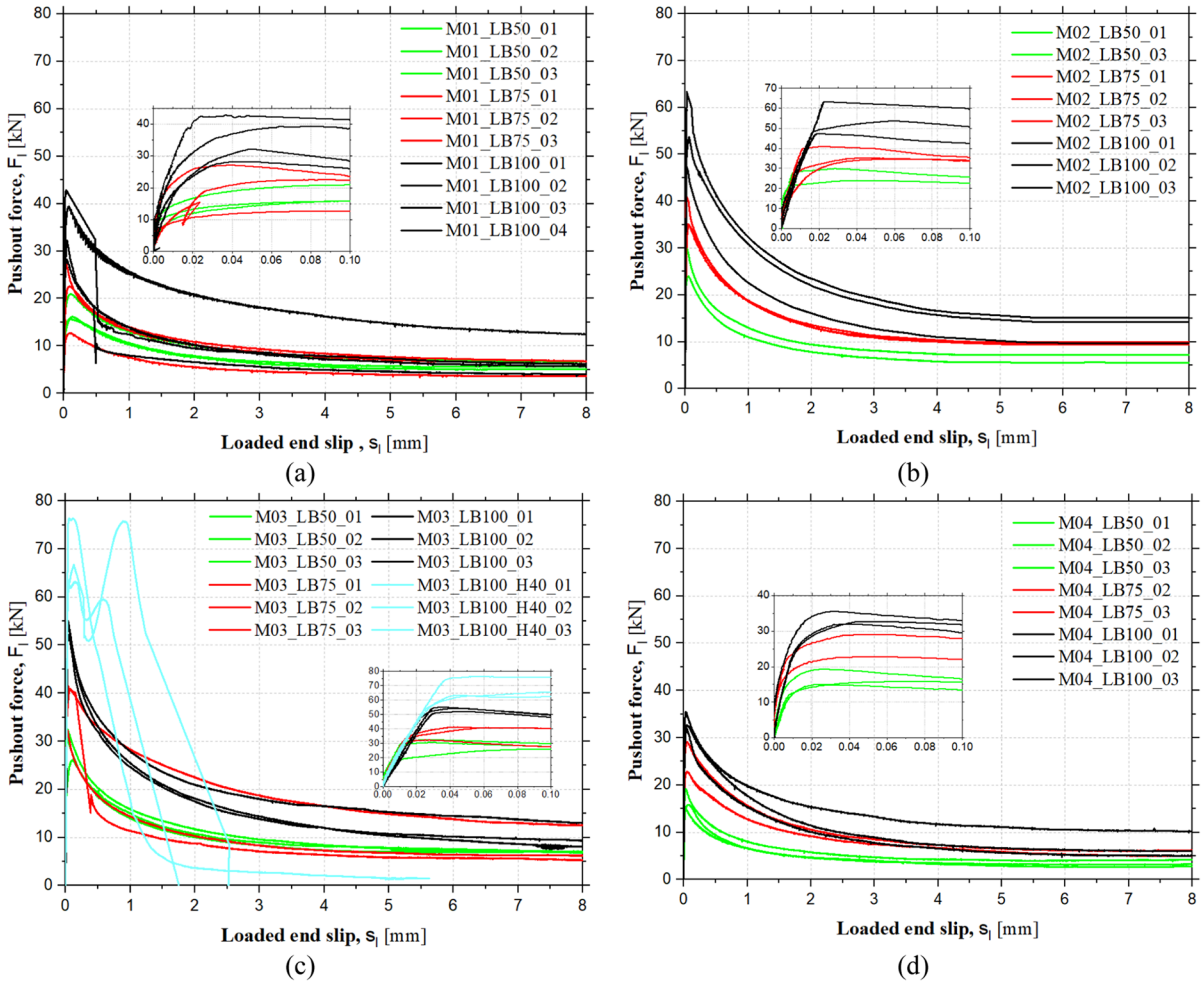

Fig. 5 F_l-s_l experimental responses: **a** M01, **b** M02, **c** M03 and **d** M04. (Color figure online)

physical contact between materials. In the post-peak phase, the bond behaviour is governed by friction, which is typical in smooth surfaces. The descending shape of the F_l–s_l post-peak response reflects the gradual degradation of the interface, which leads to the reduction of the load bearing capacity. As the loaded end slip increases and damage at the interface progresses due to friction, the force reduction tends to smooth and a residual force plateau is reached. Overall, despite slight variations between different experimental responses, the results are quite consistent and show well defined shapes. Note that tests that experienced problems during testing, were disregarded and not considered for the average results.

Table 4 summarizes the main experimental results obtained. The typical failure mode (FM) and the concrete compressive strength at 28 days ($f_{cm,28d}$) for each group series are also shown. $F_{l,\max}$ represents the maximum pushout force, $s_{l,\max}$ is the loaded end slip at maximum pushout force, $s_{f,\max}$ is the free end slip at maximum pushout force and $\tau_{\max}$ is the maximum average shear stress at the interface between the HDG steel tube and the concrete surface. The parameter F_r is the residual pushout force, defined as the pushout force obtained when s_l reaches 8 mm. G_f represents the energy dissipated during the pushout test until failure, and is obtained by computing the area under the F_l–s_l experimental curve until a s_l of 8 mm is reached. $F_r/F_{l,\max}$ is the ratio between F_r and $F_{l,\max}$.

The normalized shear strength ($\overline{\tau}_{\max}$), and the normalized energy dissipated during pushout testing until failure ($\overline{G}_f$) were computed according to

Table 4 Main pushout experimental results obtained for each mixture and series (average values)

Mixture	Series	$f_{cm,28d}$ [MPa]	$F_{l,max}$ [kN]	$s_{l,max}$ [mm]	$s_{f,max}$ [mm]	τ_{max} [MPa]	F_r [kN]	G_f [kN.mm]	$F_r/F_{l,max}$ [%]	$\overline{\tau}_{máx}$[-]	$\overline{G}_f$[-]	FM
M01	M01_LB50	20.44 [3%]	17.63 (13%)	0.11 (11%)	n.a	1.19 (12%)	5.81 (12%)	62.86 (13%)	33.06 (6%)	0.74 (12%)	0.33 (11%)	$D^{1,2,3}$
	M01_LB75		24.83 (9%)	0.07 (23%)	n.a	1.15 (6%)	6.46 (5%)	77.15 (3%)	26.11 (5%)	0.71 (6%)	0.28 (0%)	$D^{1,2,3}$
	M01_LB100		35.67 (16%)	0.05 (25%)	n.a	1.24 (14%)	7.14 (45%)	89.78 (41%)	19.78 (37%)	0.77 (14%)	0.25 (40%)	$D^{1,3,4}$ DC^{2}
M02	M02_LB50	31.17 [5%]	26.91 (11%)	0.04 (21%)	0.04 (71%)	1.76 (11%)	6.37 (13%)	60.21 (26%)	23.61 (2%)	0.72 (10%)	0.20 (25%)	$D^{1,2,3}$
	M02_LB75		36.92 (8%)	0.04 (38%)	0.04 (25%)	1.61 (8%)	9.65 (2%)	104.35 (1%)	26.29 (7%)	0.62 (1%)	0.23 (0%)	$D^{1,2,3}$
	M02_LB100		54.76 (12%)	0.03 (55%)	0.02 (47%)	1.88 (11%)	12.98 (18%)	151.13 (23%)	23.58 (10%)	0.77 (11%)	0.27 (15%)	$D^{1,2,3}$
M03	M03_LB50	37.89 [1%]	29.73 (9%)	0.05 (63%)	0.06 (69%)	2.05 (7%)	7.00 (2%)	81.51 (4%)	23.78 (11%)	0.71 (7%)	0.24 (5%)	$D^{1,2,3}$
	M03_LB75		38.20 (11%)	0.04 (31%)	0.05 (42%)	1.79 (12%)	8.18 (42%)	100.22 (38%)	21.29 (37%)	0.62 (12%)	0.20 (39%)	$D^{1,2}$ DC^{3}
	M03_LB100		55.88 (2%)	0.04 (13%)	0.05 (68%)	1.94 (1%)	10.13 (21%)	137.22 (11%)	18.81 (20%)	0.67 (1%)	0.21 (11%)	$D^{1,2,3}$
	M03_LB100_H40		71.86 (8%)	–	–	2.81 (9%)	–	89.41 (25%)	–	0.88 (9%)	–	$S^{1,2,3}$
M04 (reused tubes)	M04_LB50	43.27 [1%]	16.66 (11%)	0.04 (53%)	0.02 (45%)	1.12 (7%)	3.39 (18%)	38.56 (11%)	20.28 (10%)	0.35 (7%)	0.10 (7%)	$D^{1,2,3}$
	M04_LB75		25.94 (12%)	0.05 (4%)	0.04 (48%)	1.20 (9%)	5.61 (10%)	71.55 (8%)	21.65 (1%)	0.37 (9%)	0.13 (5%)	$D^{nd,2,3}$
	M04_LB100		33.38 (5%)	0.04 (17%)	0.04 (18%)	1.16 (2%)	7.08 (31%)	89.48 (20%)	20.94 (27%)	0.36 (2%)	0.12 (17%)	$D^{1,2,3}$

The values between parentheses are the coefficients of variation (% CoV). The upper number next to the type of FM specified the specimen with that FM

Eqs. (2), (3), respectively. The average concrete tensile strength (f_{ctm}) was estimated according to Eurocode 2 [35] and CEB-FIP Model Code [28], following Eq. (4).

$$\overline{\tau}_{max} = \frac{F_{l,\max}}{f_{ctm} \times \pi \times D \times \left(LB - S_{l,\max}\right)} \tag{2}$$

$$\overline{G}_f = \frac{G_f}{f_{ctm} \times \pi \times D \times \left(LB - S_{l,\max}\right) \times 8} \tag{3}$$

$$f_{ctm} = 0.3 \times f_{ck}^{\left(\frac{2}{3}\right)} \tag{4}$$

In a first observation to Table 4, it appears that the value of CoV is more consistent and homogeneous for $F_{l,max}$ e τ_{max}, varying between 2 and 16%, which are considered good for the type of test performed. With regard to the remaining variables, there is greater variability of results and disparity between them. For example, in the case of F_r, the minimum and maximum CoV were 2% and 45%, respectively. The remaining variables follow a similar pattern. However, and despite the CoV values being higher than desirable, they are considered acceptable and normal since some of the mechanisms related to these variables present a fragile and sensitive behaviour. Furthermore, despite all the care taken during the production of the specimens, it is important to mention that the heterogeneity of the concrete and the geometric imperfections may also have influenced this variability.

In general, based on the results presented in Table 4, there is an evident effect of the concrete mixture on the bond response values obtained. Comparing the mixtures (M01 to M03), the higher $f_{cm,\,28d}$ (M03 > M02 > M01) resulted in higher $F_{l,max}$, τ_{max} and F_r. Nevertheless, the order of magnitude of $\overline{\tau}_{max}$ and $\overline{G}_f$ were similar between groups. It was possible to identify a polynomial trend in the relationship between the compressive strength of the concrete and the bond shear stress established at the interface.

The influence on LB on the bond behaviour is less pronounced for the range of LB studied. Increasing LB led to higher $F_{l,\,max}$ in all three mixtures, as expected due to the larger contact area of the bonding interface. The same was observed for F_r and G_f. The τ and $\overline{\tau}$ values showed to be consistent among specimens of the same series, as well as among series of the same group, for all groups.

In addition, the $F_r/F_{l,max}$ ratio was consistent and values of the same order of magnitude were observed for all specimens. An average value of 23.27% was found, with a maximum of 33.06% and a minimum of 18.81%.

The clearly different results obtained for M04 when comparing to M03 show that contaminated surface do not lead to the same results. Possible causes may be the previous contact of the bond surface with cement paste, which may produce a reaction that promotes better chemical bonding the first time it occurs. When the tubes are reused, part of this effect may be lost, because the main mechanism that contributes to the bond strength is the chemical bond between the fresh concrete and the galvanized coating. The reuse of the tubes may therefore result in a weaker and less uniform bond between the materials. The results of M04 are important to show that transport and handling of HDG steel during construction must be done with care, as recommended by the associations of HDG [30], in order to fully preserve the original interface properties.

Figure 6 shows the F_l–s_l responses computed for all specimens tested, considering each bond length and concrete composition. The average responses were obtained by averaging the pushout force obtained at each loaded end slip for all specimens of the same LB and concrete strength. In general, test specimens from different groups with the same LB presented very similar F_l–s_l initial stiffnesses and overall response. Despite this, the type of concrete showed to clearly influence the load carrying capacity. Therefore, the maximum shear stress is the most affected variable when concrete strength and cement content are increased. The concrete pin adopted in the LB100_H40 specimens influenced the shape and magnitude of the values obtained in the experimental response, especially in the post-peak phase, and softening was not gradual as in the other cases (Fig. 6d).

3.2 Failure modes

Figure 7 shows representative images of the most frequently FM. In general three different failure modes were observed:

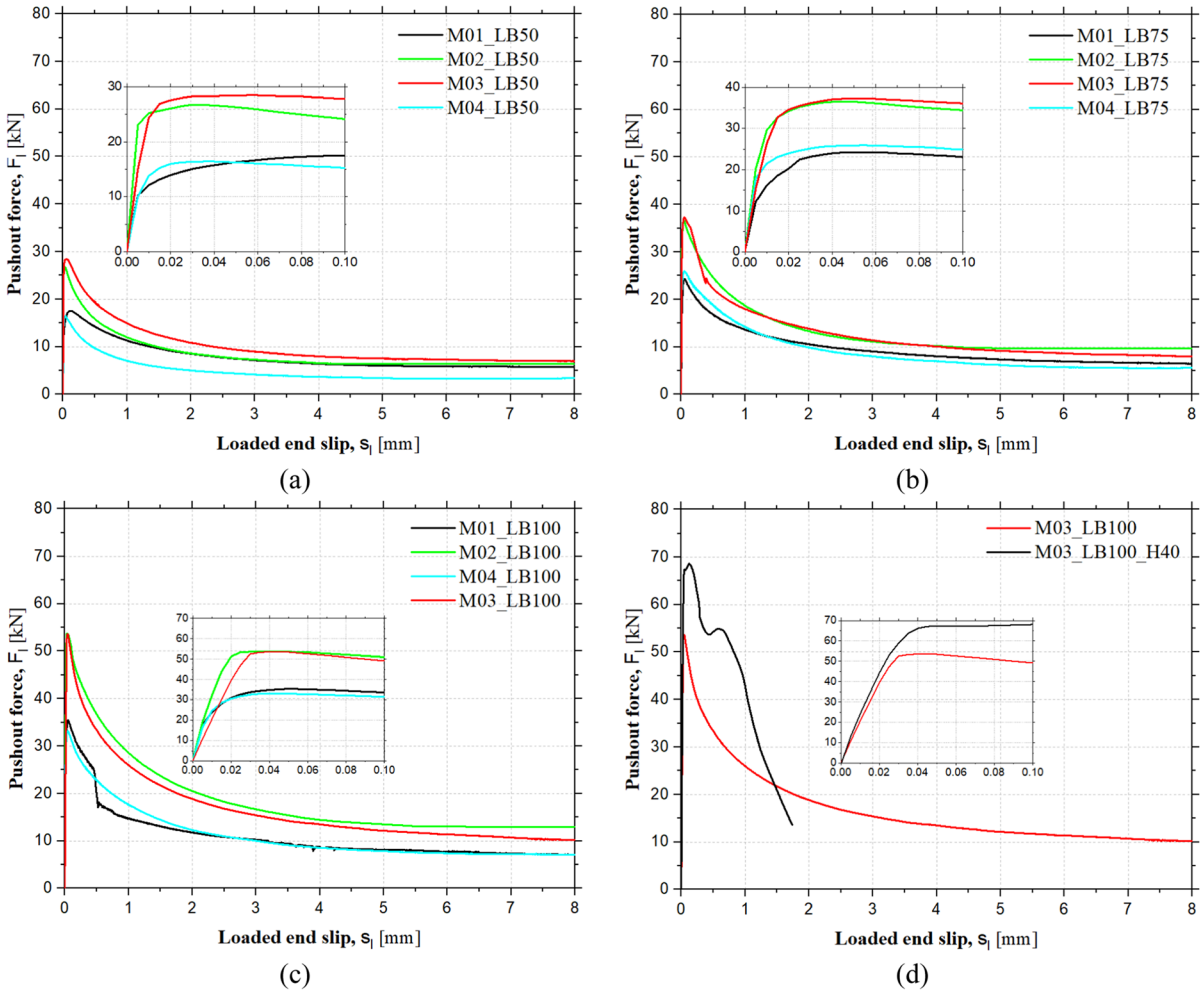

Fig. 6 Average pushout force versus loaded end slip ($Fl-sl$) responses computed for all specimens tested: **a** LB50, **b** LB75, **c** LB100 and **d** LB100 vs LB100_H40. (Color figure online)

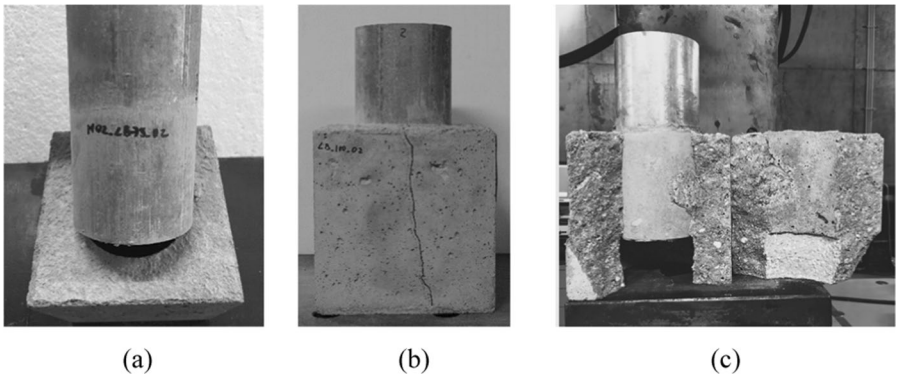

Fig. 7 Failure modes: **a** D, **b** DC and **c** S

- D—pushout debonding failure at the concrete to HDG steel tube interface, which consists on the full development of a tunnel crack at the interface between both materials and the slipping of the steel tube with respect to the concrete block. This was the most common failure mode, which indicates an appropriate concrete substrate behaviour and the objective characterization of the bond behaviour. After removing the HDG steel tubes from the concrete substrates, homogeneous cement bonding films were visible at the surface of the tubes, as well as friction marks (Fig. 7a);
- DC—formation of a thin crack in the concrete block during pushout debonding failure, visible after $F_{l,\max}$ is reached (Fig. 7b). Given the reduced crack opening, a colour line adjacent to the crack was used to better identify the crack path. The surrounding concrete was not able to accommodate the tensile stresses generated during the push-out test, possibly influenced by a small vertical misalignment of the tube. Specimens M01_LB100_02 and M03_LB75_03 cracket during testing, and a sudden decrease in the F_l was observed. Despite that, the experimental F_l–s_l responses showed a similar overall shape when compared to the specimens with debonding failure (*D*). Note that M04_LB75_01 showed a crack even before testing, probably caused by any accidental impact. An homogeneous cement bonding films were also visible at the steel surface.
- S—premature failure of the concrete block by splitting (Fig. 7c). This failure mode was observed for the specimens M04_LB100_H40 and occurs due to excessive radial tensile stresses originated by the pushout load transfer from the HDG steel tube to the concrete block, which results in cracks in the transverse and longitudinal directions. The pushout behaviour is determined by the characteristics of concrete block itself and not by the bond properties, therefore the $F_{l,\max}$ is underestimated. In this case, the obtained experimental responses were quite different. After reaching a maximum load value, which was higher than in the specimens of the same type without holes, the concrete cubes suffered splitting failure, resulting in an abrupt drop in the load carrying capacity to 0 kN. The size of the concrete cubes would have to be substantially increased in order to avoid premature failure of the concrete block and allow full mobilization of the maximum bond strength. This means that, although a higher bond strength was obtained, the values could be even higher if the concrete blocks remained intact.

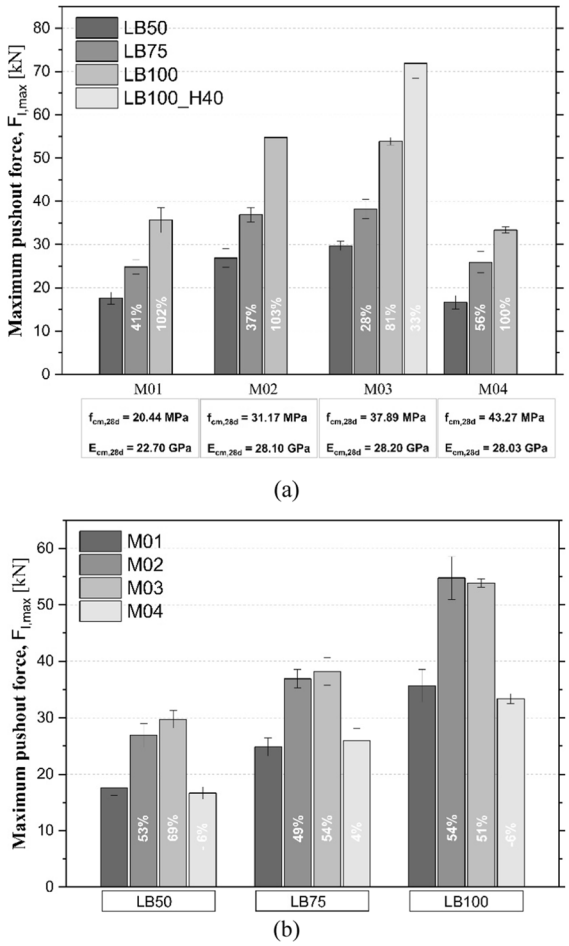

Fig. 8 Influence of the concrete strength, M01 to M04 (**a**), and LB (**b**), on the average value of $F_{l,\max}$ within each series

3.3 *Maximum pushout force ($F_{l,max}$)*

Figure 8 shows the average results obtained in terms of $F_{l,\max}$ with respect to concrete strength (Fig. 8a) and the bond length (Fig. 8b). The values within the bars represent the percentage increase compared to the first bar's value. LB100_H40 was compared to LB100.

For M01, $F_{l,\max}$ increased by + 41% when comparing LB50 and LB75, and + 102% when LB50

and LB100 are compared. In the case of M02, when comparing LB50 to LB75 and LB50 to LB100, the increase was + 37% and + 103%, respectively. For M03, the increase was about + 28% and + 81% when comparing LB50 to LB75 and LB50 to LB100, respectively. Furthermore, the specimens LB100_H40 experienced an increase of + 33% when compared to LB100. Regarding M04, the increase was + 56% and + 100% for the same bond lengths comparison. In summary, it was found that for the different series the maximum pull-out force, $F_{l,\max}$, was approximately proportional to the bond length.

Figure 8b shows that the parameters obtained in the tests were also clearly influenced by the concrete mixture and the cement content. For LB50, with respect to M01 a variation of $F_{l,\max}$ of + 53%, + 69% and − 6% for mixtures M02, M03 and M04, respectively, was obtained. In the case of LB75, the variation of $F_{l,\max}$ was + 49%, + 54% and + 4%. For LB100, a variation of + 54%, + 51% and − 6% was found. Summarizing, for all the three LB a significant increase in $F_{l,\max}$ was found when M01 and M02 are compared. Between M02 and M03 this increase was less significant. In the case of M04, the values were very similar to those of M01.

3.4 *Maximum shear stress (τ_{max})*

Despite slight variations, the $\tau_{\max}$ and the $\overline{\tau}_{\max}$ values for the various LB of the same concrete mixture were quite similar and consistent, as shown in .

a. The average value of $\tau_{\max}$ referring to the average obtained from all LBs of the same concrete mixture were also computed. In the case of M01, $\tau_{\max}$ averaged 1.19 ± 0.04 MPa (± 3%). Comparing LB75 and LB100 to LB50, variations were −4% and + 4%, respectively. For M02, $\tau_{\max}$ averaged 1.75 ± 0.11 MPa (± 6%), with variations of − 9% and + 7%. For M03, the averaged of $\tau_{\max}$ was 1.93 ± 0.11 MPa (± 6%), with variations of − 13% and − 5%. Comparing LB100 to LB100_H40, a significant increase of + 45% in $\tau_{\max}$ was observed, suggesting improved adherence promoted by the concrete pin. In M04, the average value of $\tau_{\max}$ was 1.16 ± 0.03 MPa (± 3%), with variations of + 7% and + 4%. $\tau_{\max}$ occurred at loaded end slips between 0.04 mm (most common) and 0.11 mm. In terms of $\overline{\tau}_{max}$, a mean value of 0.74 ± 0.02 (± 3%), 0.70 ± 0.06 (± 9%), 0.67 ± 0.04 (± 6%) and 0.36 ± 0.01 (± 3%) was found for the specimens of M01, M02, M03 and M04, respectively (Fig. 9c). The $\tau_{\max}$ experimentally obtained for a particular LB would require a higher LB in order to meet the maximum 'theoretical' value. The relations between LB, f_{cm} and $\tau_{\max}$ indicating that the LBs adopted are lower than the effective LB (Fig. 9e, f).

The concrete strength influenced the $\tau_{\max}$, regardless of the LB. An average variation of 53.8% was found considering M01 to M03, with a maximum of + 72% (Fig. 9b). Despite the variations noted, the $\tau_{\max}$ showed increasing values for the specimens of mixtures M03 > M02 > M03, which corresponded to the increase in the concrete compressive strength ($f_{cm,M03} > f_{cm,M02} > f_{cm,M01}$). The increasing of f_{cm} results in a polynomial increase in the experimental bond stress, although the theoretical values show linear increase.

M04 presented identical values of $\tau_{\max}$ to those of M01 showing that the surface contamination significantly reduced the bond stress in around − 39.5% (M04 to M03), equivalent to a reduction in the concrete's compressive strength of 53% (Fig. 9e, f). Considering the mechanical parameters of the concrete mixtures presented in Table 3, it was found that the mixture M02 was superior to M01 both in terms of compressive strength (52%) and modulus of elasticity (+ 24%). M03 was superior in 113% and + 23% and, M04 in + 85% and + 24% in terms of $f_{cm,28d}$ and $E_{cm,28d}$, respectively.

Concretes with a higher resistance results in a better chemical bond strength in a polynomial relationship. Although these trend was observed between M01, M02 and M03, the same did not occur between M04 (reused tube) and M01. In this case, the values of $F_{l,\max}$ and $\tau_{\max}$ were very similar despite its superiority in the f_{cm}. However, looking at the homogenized variables, it appears that the values obtained for M04 are about half of those mixtures, and this difference cannot be neglected (Fig. 9d). Independently of LB and contrary to what happened for $\tau_{\max}$, the specimens of M01 resulted in $\overline{\tau}_{\max}$ values higher than those obtained for M04, which highlights the importance of normalizations of the variables. Despite small variations, the values of $\overline{\tau}_{\max}$ are all approximate.

3.5 *Energy dissipated (G_f)*

The total energy is clearly influenced by both LB (Fig. 10a) and the concrete mixture (Fig. 10b).

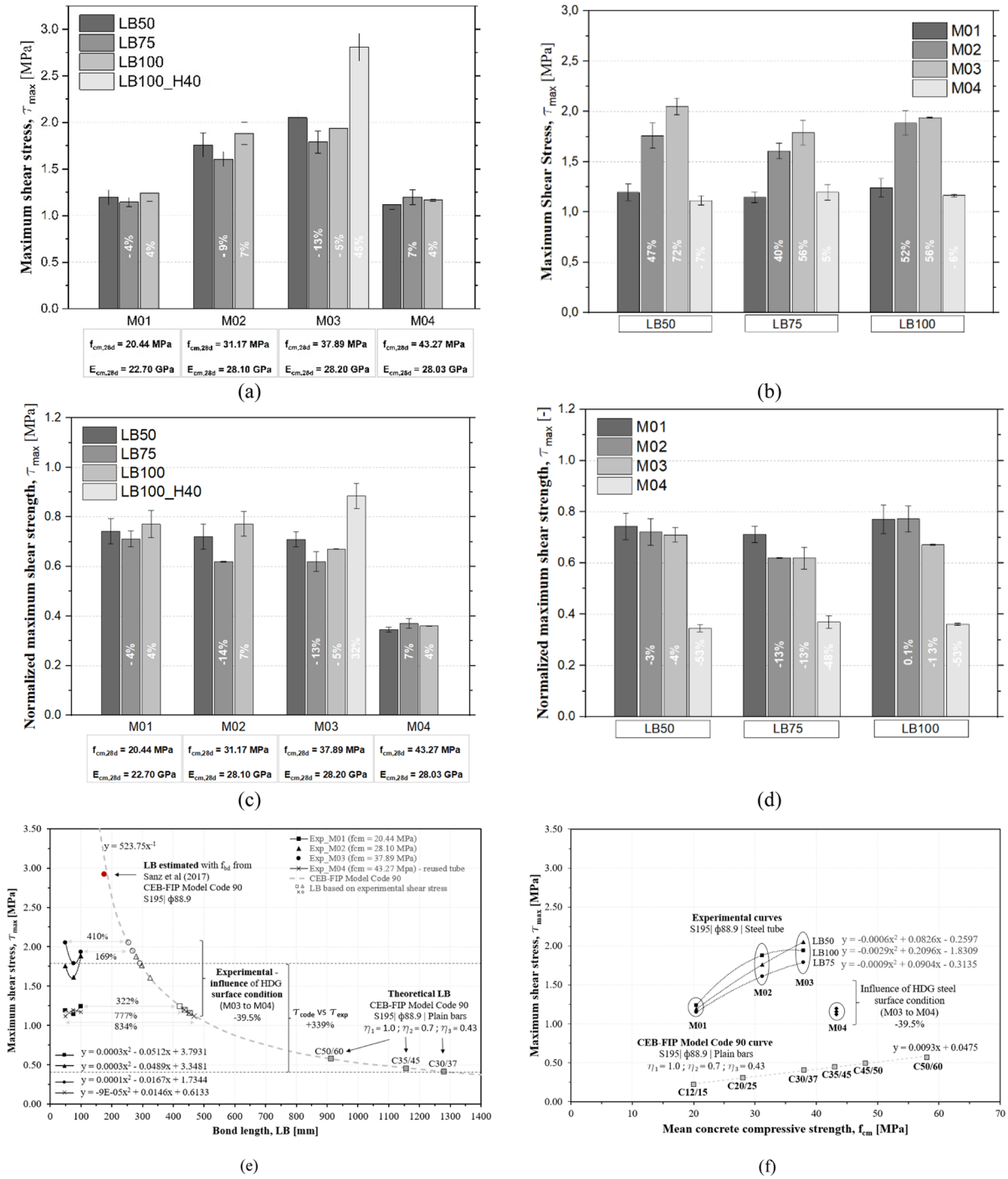

Fig. 9 Influence of the f_{cm} and LB, on the average values of τ_{max} (**a**, **b**, **e**, **f**), and $\overline{\tau}_{max}$ (**b**, **d**), within each series

In the case of the mixture M01, there was a + 23% and + 43% variation between LB50 and LB75 and between LB50 and LB100, respectively. In mixture M02 the variation was + 73% and + 151%. In the case of M03, the variation was + 23% and + 69%. In mixture M04 there was a variation of + 86% and + 132%.

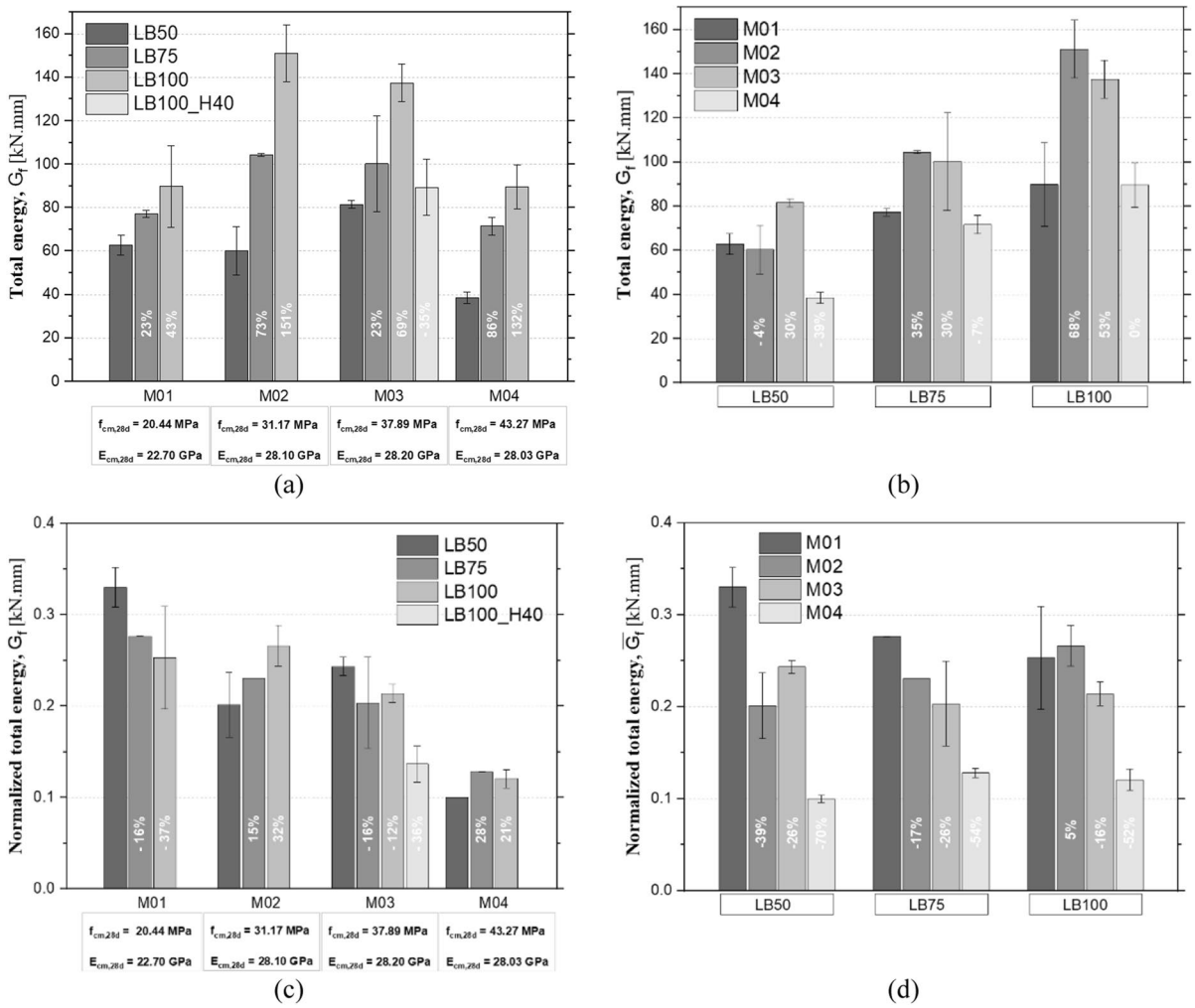

Fig. 10 Influence of the type of concrete and LB, on the average values of the energy dissipated during pushout testing, G_f (**a**, **b**), and $\overline{G}_f$ (**c**, **d**), within each series. Residual force (F_r)

The LB value was found to have greater influence on total energy in mixtures M02 and M04 and less influence in mixtures M01 and M03. In the case of LB100_H40, the specimen presented a fragile rupture and as a consequence the total energy was affected. Although the type of concrete influences the total energy, it should be noted that the variations were smaller than those found on the influence of anchorage length. In general, apart from LB50, the specimens for mixture M02 had a higher total energy. Regarding to normalized energy, it appears that the values were similar between all groups, with a mean value of 0.245 (Fig. 10c, d).

Figure 11 shows that the residual force raise with higher values of LB, regardless of the concrete type mixture. The results also show a greater increase in residual strength for higher strength concrete, except for M04. While in the M01 mixture the increase between LB50 and LB75 was + 11% and between LB50 and LB100 was + 23%, in the case of mixtures M02 and M04 the increments were more than double. In M02 there was an increase of + 52% and + 104% and in the case of M04 a variation of + 65% and + 109% was observed. For M03, a variation of + 17% and + 45% was found. Note that the F_r obtained for the series LB100_H40 was near 0 kN,

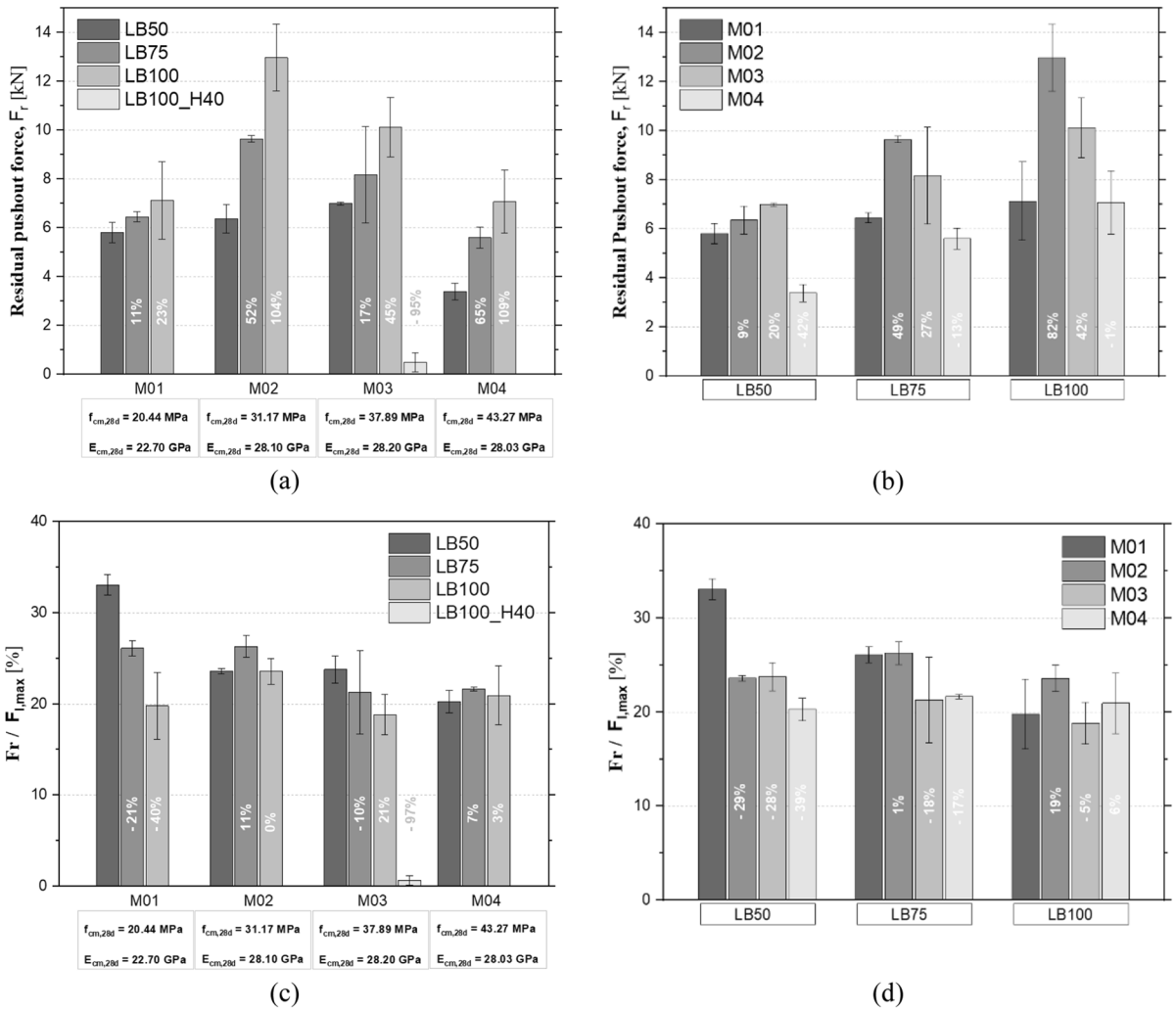

Fig. 11 Influence of the type of concrete, M01 to M04, and of LB, on the average values of F_r, (**a**, **b**), and $F_r/F_{l,\max}$ (**c**, **d**), within each series

which was expected considering the brittle type of rupture observed.

The highest residual strength values were obtained for the M02 with a value of 12.98 kN for the series LB100. The lowest values correspond to the M04, series LB50, with a value of 3.39 kN.

In addition, the $F_r/F_{l,\max}$ ratio was consistent and the values present the same order of magnitude for all specimens. Thus, considering all the specimens, an average value of $F_r/F_{l,\max}$ equal to + 23.3% was found, with a maximum of 33.1% and a minimum of 18.8%.

According to the literature, the three main mechanisms that influence bond strength are [23]: (i) the coating itself, (ii) the chemical reaction between zinc and the wet cement paste and (iii) the retarding effect of corrosion products that result from the reaction of zinc with the wet cement paste on cement hydration. As noted, the chemical component is an important mechanism that can actively influence the bond strength. The alkaline environment of the fresh concrete activates the galvanized steel surface, and zinc layer corrodes until passivation occurs. Since only one type of coating was used in this work for four different concrete mixtures, it is natural that different

reaction products are formed. Thus, this may justify the variations observed for test specimens of different mixtures but with the same LB. Indeed, the concrete mixture seems to provide more influence on the results than the anchorage length.

It is important to emphasize the importance and care that must be taken when working with composite systems made of concrete and galvanized steel in order to prevent involuntarily contamination of the galvanized surface Although not intentionally, the existence of contaminating products such as oils and their variants resulting from the handling, transportation and application on site of this type of material can cause a decrease in the adherence between the materials, as stated by the American Galvanizers Association, that also educates on how to deal and decontaminate possible contaminated surfaces.

4 Conclusions and future works

This sub-chapter summarized the results obtained in an experimental program composed by 40 pushout tests performed in concrete cubes reinforced with HDG steel tubes, 32 cylinders to characterize concrete mixtures and 4 steel specimens to characterize the mechanical properties.

The results obtained led to the following main conclusions:

1. The behaviour of all the tested specimens was consistent and similar to those obtained by Sanz et al. (2017): the curves showed a positive initial steep slope, as a result of the high stiffness of the system due to the strong bond between the two materials, raising up to $F_{l,\max}$ and then progressively descend to a residual stress plateau.
2. LB and concrete mixture did not significantly influence the shape of the curve $F_l - s_l$, however both influenced the values obtained of $F_{l,\max}$, G_f and F_r.
3. Higher f_{cm} led to a higher $\tau_{\max}$ in a polynomial relationship;
4. The $\tau_{\max}$ experimentally obtained for a particular LB would require a higher LB in order to meet the maximum 'theoretical' value, depending on the concrete strength. The relations between LB, f_{cm} and $\tau_{\max}$ indicating that the LBs adopted were significantly lower than the effective LB;
5. The importance of a clean HDG surface, in contrast to a contaminated surface, is clear on the results as the later reduces bonding in −39.5%, which may be equivalent to a reduction in the concrete's strength of 53%;
6. The failure mode observed was consistent. Debonding (*D*), debonding with crack (DC) an splitting (*S*) were observed. Debonding phenomenon was the main FM, as expected.
7. The contribution of the concrete pin achieved through the pipe hole improved the adhesion between materials. It should be noted, however, that the global failure mode was not the desired one and that the adherence bond stress could be even higher than that obtained.
8. The test specimens and the methodology adopted proved to be adequate to fully characterize the bond behaviour between HDG steel tube and concrete.

Finally, the present study represents a first step for an extended investigation to study the effect of seawater on bond behaviour over time for marine applications. Some of the aspects to be considered include environmental factors' effect or the corrosion mechanism in bond behaviour (durability). Microstructural analysis with chemical assessment of the HDG coating–concrete interface could also help to clarify some of the bond mechanisms established during curing and corrosion process. Investigate the constitutive model of bond-slip and include it in analytical and numerical models."

Acknowledgements The financial supports of Fundação para a Ciência e Tecnologia (FCT) co-supported by European Social Fund (FSE) [grant number SFRH/BD/137220/2018]; and of Comissão de Cordenação e Desenvolvimento Regional do Norte (CCDR-N) and Fundo Europeu de Desenvolvimento Regional (FEDER) within the research project ''NEXTSEA" [grant number NORTE-01-0145-FEDER-000032] are gratefully acknowledged.

Funding Open access funding provided by FCT|FCCN (b-on).

Declarations

Conflict of interest The authors declare that they have no conflict of interest.

Open Access This article is licensed under a Creative Commons Attribution 4.0 International License, which permits

use, sharing, adaptation, distribution and reproduction in any medium or format, as long as you give appropriate credit to the original author(s) and the source, provide a link to the Creative Commons licence, and indicate if changes were made. The images or other third party material in this article are included in the article's Creative Commons licence, unless indicated otherwise in a credit line to the material. If material is not included in the article's Creative Commons licence and your intended use is not permitted by statutory regulation or exceeds the permitted use, you will need to obtain permission directly from the copyright holder. To view a copy of this licence, visit http://creativecommons.org/licenses/by/4.0/.

References

1. Liu PC (1991) Damage to concrete structures in a marine environment. Mater Struct 24(4):302–307. https://doi.org/10.1007/BF02472086
2. Cruz F, Pereira E, Valente IB, Tiago M, Maslov D, Pinheiro M,(2018) Structural design of an innovative multifunctional artificial reef. In: Oceans 2018 MTS/IEEE Charleston, Charleston: IEEE, pp. 1–7. https://doi.org/10.1109/OCEANS.2018.8604587.
3. Ragab AM, Elgammal MA, Hodhod OAG, Ahmed TES (2016) Evaluation of field concrete deterioration under real conditions of seawater attack. Constr Build Mater 119:130–144. https://doi.org/10.1016/j.conbuildmat.2016.05.014
4. Shi X, Xie N, Fortune K, Gong J (2012) Durability of steel reinforced concrete in chloride environments: an overview. Constr Build Mater 30:125–138. https://doi.org/10.1016/j.conbuildmat.2011.12.038
5. González JA, Vazquez AJ, Jauregui G, Andrade C (1984) Effect of four coating structures on corrosion kinetic of galvanized reinforcement in concrete. Matériaux Constr 17(6):409–414. https://doi.org/10.1007/BF02473980
6. Figueira RB, Silva CJR (2014) Corrosion of hot-dip galvanized steel reinforcement. Corros Prot Mater 33(3):51–61
7. Coccia S, Imperatore S, Rinaldi Z (2016) Influence of corrosion on the bond strength of steel rebars in concrete. Mater Struct Constr 49(1–2):537–551. https://doi.org/10.1617/s11527-014-0518-x
8. Baltazar-Zamora MA et al (2019) Corrosion behaviour of galvanized steel embedded in concrete exposed to soil type MH contaminated with chlorides. Front Mater 6:1–12. https://doi.org/10.3389/fmats.2019.00257
9. Tej P, Kour M, Pokorny P (2017) Evaluation of the impact of corrosion of hot-dip galvanized reinforcement on bond strength with concrete—a review. Constr Build Mater 132:271–289. https://doi.org/10.1016/j.conbuildmat.2016.11.096
10. Rivera-Corral JO, Fajardo G, Arliguie G, Orozco-Cruz R, Deby F, Valdez P (2017) Corrosion behaviour of steel reinforcement bars embedded in concrete exposed to chlorides: effect of surface finish. Constr Build Mater 147:815–826. https://doi.org/10.1016/j.conbuildmat.2017.04.186
11. Hellio C, Yebra D (2009) Advances in marine antifouling coatings and technologies. Elsevier, Burlington
12. Sena-Cruz J, Cunha VMCF, Camões A, Barros JAO, Cruz P (2009) Modelling of bond between galvanized steel rebars and concrete. In Congresso de Métodos Numéricos em Engenharia 2009:1–15
13. Yu Z, Hu J, Meng H (2020) A review of recent developments in coating systems for hot-dip galvanized steel. Front Mater 7:1–19. https://doi.org/10.3389/fmats.2020.00074
14. Yeomans SR (2019) Galvanized reinforcement in bridge and coastal construction, In: 20th Congress of IABSE, New York City, pp. 1592–1598
15. Arguillarena A, Margallo M, Urtiaga A, Irabien A (2021) Life-cycle assessment as a tool to evaluate the environmental impact of hot-dip galvanisation. J Clean Prod 290:125676
16. Wang F, Cheng Z, Shen J (2023) Flexural fatigue behaviour of butt-welded circular concrete-filled double skin steel tube (CFDST): Experimental study and numerical modelling. Mar Struct 88:103380
17. Tao Z, Song TY, Uy B, Han LH (2016) Bond behaviour in concrete-filled steel tubes. J Constr Steel Res 120:81–93. https://doi.org/10.1016/j.jcsr.2015.12.030
18. Chen Z, Zhou J, Ban M, Wang X (2020) Residual bond behaviour of steel reinforced recycled aggregate concrete after exposure to elevated temperatures. Front Mater 7:1–16. https://doi.org/10.3389/fmats.2020.00142
19. Hamad BS, Mike JA (2005) Bond strength of hot-dip galvanized reinforcement in normal strength concrete structures. Constr Build Mater 19:275–283. https://doi.org/10.1016/j.conbuildmat.2004.07.008
20. Tittarelli F, Bellezze T (2010) Investigation of the major reduction reaction occurring during the passivation of galvanized steel rebars. Corros Sci 52(3):978–983. https://doi.org/10.1016/j.corsci.2009.11.021
21. Maeda M, Li X, Ooi A, Tada E, Nishikata A (2020) Passivation mechanism of galvanized steel rebar in fresh concrete. ISIJ Int 60(2):337–345. https://doi.org/10.2355/isijinternational.ISIJINT-2019-396
22. Blanco MT, Andrade C, Macias A (1984) SEM study of the corrosion products of galvanized reinforcements immersed in solutions in the pH range 12·6–13·6. Br Corros J 19(1):41–48. https://doi.org/10.1179/000705984798273524
23. Yeomans SR (2004) Galvanized steel reinforcement in concrete. Elsevier, Amsterdam
24. Pokorný P, Pernicová R, Tej P, Kolísko J (2019) Changes of bond strength properties of hot-dip galvanized plain bars with cement paste after 1 year of curing. Constr Build Mater 226:920–931. https://doi.org/10.1016/j.conbuildmat.2019.07.147
25. Ortolan VDK, Hilgert T, Howland JJ, Silva L, Titikian BF (2017) Comparative assessment of corrosion of concrete reinforced with unprotected steel and hot-dip galvanized steel. Rev la Construcción J Constr 16(2):238–248. https://doi.org/10.7764/RDLC.16.2.238
26. Javier F, Molina L, Cruz M, Alonso A, Montes EH, Cecilio L (2017) Galvanized steel in concrete: more durable structures maintaining the bond length. J Mater

Civ Eng. https://doi.org/10.1061/(ASCE)MT.1943-5533.0001903
27. Sun G, Yang K (2023) Bond-slip behaviour between multi-partition steel tubes and concrete. Mater Struct Constr 56(3):1–13. https://doi.org/10.1617/s11527-023-02155-3
28. Comite Euro-International du Beton (2016) Bullettin d'information 213/214 - CEB-FIP Model Code 1990
29. Andreasen AHM, Andersen J (1930) Ueber die beziehung zwischen kornabstufung und zwischenraum in produkten aus losen körnern (mit einigen experimenten). Kolloid-Zeitschrift 50(3):217–228. https://doi.org/10.1007/BF01422986
30. American Galvanizers Association (2023) Hot-dip galvanizing - preparing the HDG surface, American Galvanizers Association, Colorado. https://galvanizeit.org/duplex-systems-galvanize-it-seminar/preparing-the-hdg-surface (accessed Apr. 14, 2023).
31. EN 12350-2 (2009) Testing fresh concrete-part 2: slump-test. European standard, p. 8,
32. EN 12390-1, Testing hardened concrete–part 1: shape, dimensions and other requirements for specimens and moulds. In: European standard, Brussels, Belgium, 2012, p. 14.
33. EN 12390-13 (2013) Testing hardened concrete part 13 : determination of secant modulus of elasticity in compression, European standard. Brussels, Belgium, p. 14
34. EN 12390-3 (2009) Testing hardened concrete-part 3: compressive strength of test specimens, European standard. p. 21
35. EN 1992-1-1 (2004) Eurocode 2: design of concrete structures - part 1-1: general rules and rules for buildings, European standard. Brussels, Belgium, p. 225
36. ISO 6892-1 (2009) Metallic materials—tensile testing—part 1: method of test at room temperature 1, International standart, vol 2009, p. 72
37. Sanz B, Planas J, Sancho JM (2017) Study of the loss of bond in reinforced concrete specimens with accelerated corrosion by means of push-out tests. Constr Build Mater 160:598–609. https://doi.org/10.1016/j.conbuildmat.2017.11.093
38. Joana Azevedo Gonçalves (2021) Mixed galvanized steel and concrete systems for the construction of marine and offshore structures, University of Minho. [Online]. Available: [in Portuguese]

Publisher's Note Springer Nature remains neutral with regard to jurisdictional claims in published maps and institutional affiliations.